Measuring Faraday Complexity

Cormac Purcell, Jennifer West and the POSSUM team

May 19, 2017

Abstract

Here we present proposed methods for measuring complexity in polarised sources. These methods are currently implemented in the prototype POSSUM pipeline, written by Cormac Purcell and available at https://github.com/crpurcell/RM-tools. This document is a work-in-progress and is intended to foster discussion in the POSSUM Survey Groups 5 & 8.

1 Faraday Rotation

Faraday rotation causes the polarisation angle ψ of a linearly polarised wave to be rotated when passing through a magnetised parcel of ionised gas. The change in polarisation angle is a function of wavelength and is given by

$$\Delta\psi = \phi\,\lambda^2 \quad \text{rad}, \tag{1}$$

where ϕ is the Faraday depth in radians m^{-2} and λ is the wavelength of the emission. In the simple case of a purely rotating 'Faraday thin' medium, ϕ is constant with λ^2 and is known as the rotation measure (RM). Observationally, RM is easily determined from a linear fit to ψ versus λ^2. Physically, RM is related to the line-of-sight component of the magnetic field strength $B_{||}$ and the thermal electron density n_e via

$$\text{RM} = \left[\frac{e^3}{2\pi m_e^2 c^4}\right] \int_{src}^{obs} n_e\, B_{||}\, \text{d}l \quad \text{rad}\,\text{m}^{-2}, \tag{2}$$

where the integral is taken from the source to the observer along the path length $\text{L} = \int \text{d}l$ through the ionised medium. Positive RM indicates an average magnetic field pointing out of the plane of the sky. If n_e and L are known (e.g., from independent observations and the geometry of the ionised gas), then $B_{||}$ can be estimated. The constant in square brackets has a value of ~ 0.81 if $B_{||}$ is in units of μG, n_e in cm^{-3} and L in pc. If the ionised material is clumpy, $\int \text{d}l$ is characterised by the occupation length fL, where f is the volume filling factor.

2 Faraday complexity

Observed structures are often much more complicated than the simple Faraday rotating medium outlined in §1. Signals from multiple clumps of Faraday-active material can mix together to produce complex behaviour in the polarised spectra. Additional complexity is introduced if the intervening gas is also emitting polarised synchrotron radiation. In these 'Faraday thick' scenarios, both the polarisation angle ψ and Faraday depth ϕ become non-linear functions of λ^2. Faraday depth is no longer a constant, making the task of reconstructing the magneto-ionic properties challenging.

3 Detecting Faraday complexity

Faraday complexity can arise from a multitude of different physical scenarios (e.g., see Farnes et al. 2014) and testing for all of these would be impossible. It is much simpler to ask: *Is the data consistent with a Faraday*

thin scenario?. Two approaches to answering this question are used in the prototype POSSUM pipeline[1]. The first method operates directly on the Stokes I Q & U spectra and tests whether the distribution of values deviate from that expected for a Faraday thin component. The second method tests if the Faraday depth dispersion of $|\mathcal{F}(\phi)|$ is significant compared to the width of Rotation Measure Spread Function (RMSF).

3.1 Detecting complexity in a polarised spectrum

We start by performing RM-synthesis on the fractional $q(\lambda^2)$ and $u(\lambda^2)$ spectra to form the complex Faraday dispersion function $\mathcal{F}(\phi)$. We measure the Faraday depth $\phi_{\rm peak}$, intrinsic polarisation angle ψ_{λ_0} and fractional polarisation p of the peak in $|\mathcal{F}(\phi)|$ and create a model Faraday thin spectrum $\mathcal{P}(\lambda^2) = p\,e^{2i\,(\psi_{\lambda_0} + \phi_{\rm peak}\,\lambda^2)}$. The real and imaginary components of this model spectrum are subtracted from the data to form residual $q_{\rm res}(\lambda^2)$ and $u_{\rm res}(\lambda^2)$ spectra. Assuming an accurate Stokes I model and normally distributed uncertainties, any unexpected structure in the residual spectra will be indicative of Faraday complexity.

Depolarisation mechanisms preferentially effect the long wavelength end of the spectrum (see Tribble 1991, Sokoloff et al. 1998 and Brentjens & de Bruyn 2005), however, spectral structure can also be introduced across the pass-band via mixing between multiple polarised signals. To avoid making assumptions about how complexity manifests in the spectrum, we model structure in the residual as a wavelength-independent noise term $\sigma_{\rm add}$ that increases the scatter of the data according to

$$\sigma^2_{{\rm total},i} = \sigma^2_{{\rm noise},i} + \sigma^2_{\rm add}, \tag{3}$$

where $\sigma_{{\rm noise},i}$ is the uncertainty on the $i^{\rm th}$ spectral channel. This approach has been most recently used by Allison et al. (2017) to model quasar variability and by Purcell et al. (2015) to account for poorly determined uncertainties in RM measurements. Assuming a normal distribution centred around μ, the likelihood function for $\sigma_{\rm add}$ is given by

$$\mathcal{L}(\sigma_{\rm add}) \equiv \boldsymbol{p}(d|\sigma_{\rm add}, \sigma_{\rm noise}) \propto \int \frac{1}{\sqrt{(2\pi)^N \prod_i^N \sigma^2_{{\rm total},i}}} \exp\left(-\frac{\chi^2}{2}\right) {\rm d}\sigma_{\rm add}. \tag{4}$$

If $d = [d_i \ldots, d_N]$ is the set of values with measured uncertainties $\sigma_{\rm noise} = [\sigma_i \ldots, \sigma_N]$, then $\chi^2 = \sum_i^N (d_i - \mu)^2/\sigma^2_{{\rm total},i}$, with $\mu = 0$ expected for the residual spectrum. By Bayes' theorem, the posterior probability density $\boldsymbol{p}(\sigma_{\rm add}|d, \sigma_{\rm noise})$ can be calculated by multiplying $\mathcal{L}(\sigma_{\rm add})$ by a suitable prior function $\pi(\sigma_{\rm add})$. Since we are ignorant of the value of $\sigma_{\rm add}$ we use a scale-invariant Jeffreys' prior:

$$\pi(\sigma_{\rm add}) \propto \begin{cases} \sigma_{\rm add}^{-1}, & \text{if } \sigma_{\rm add} > \langle\sigma_{\rm total}\rangle/1^3. \\ 0, & \text{otherwise.} \end{cases} \tag{5}$$

In practice we set $d(\lambda^2) = u/\sigma_u$ or q/σ_q and $\sigma_{\rm noise}(\lambda^2)$ to a unit vector so that the value of $\sigma_{\rm add}$ is normalised and comparable between disparate spectra.

Fig. 1 shows the normalised residual $u_{\rm res}/\sigma_u(\lambda^2)$ and $q_{\rm res}/\sigma_q(\lambda^2)$ for a synthetic Faraday thin spectrum (*top-left*). The distribution of values (*middle column*) is consistent with being drawn from a normal distribution. We use Eqn. 4 to calculate the marginal posterior probability distribution over a suitable range of $\sigma_{\rm add}$ values (*right column*) and report the mean of the posterior distribution as the best estimate of $\sigma_{\rm add}$. In this Faraday thin case $\sigma_{\rm add}$ is consistent with zero. Fig. 2 displays the normalised residual spectrum, distribution of values and posterior probability distribution for a Faraday complex source. The distribution of values deviates significantly from Gaussian and the posterior distribution strongly constrains the additional scatter required model the data to $\sigma_{\rm add,q} = 2.13^{+0.19}_{-0.17}$ and $\sigma_{\rm add,u} = 1.74^{+0.17}_{-0.15}$. Because we calculate $\mathcal{L}$ for the normalised residual, $\sigma_{\rm add}$ is a unitless quantity whose value may be easily compared between datasets.

[1] https://github.com/crpurcell/RM-tools and https://github.com/crpurcell/RMpipeL5

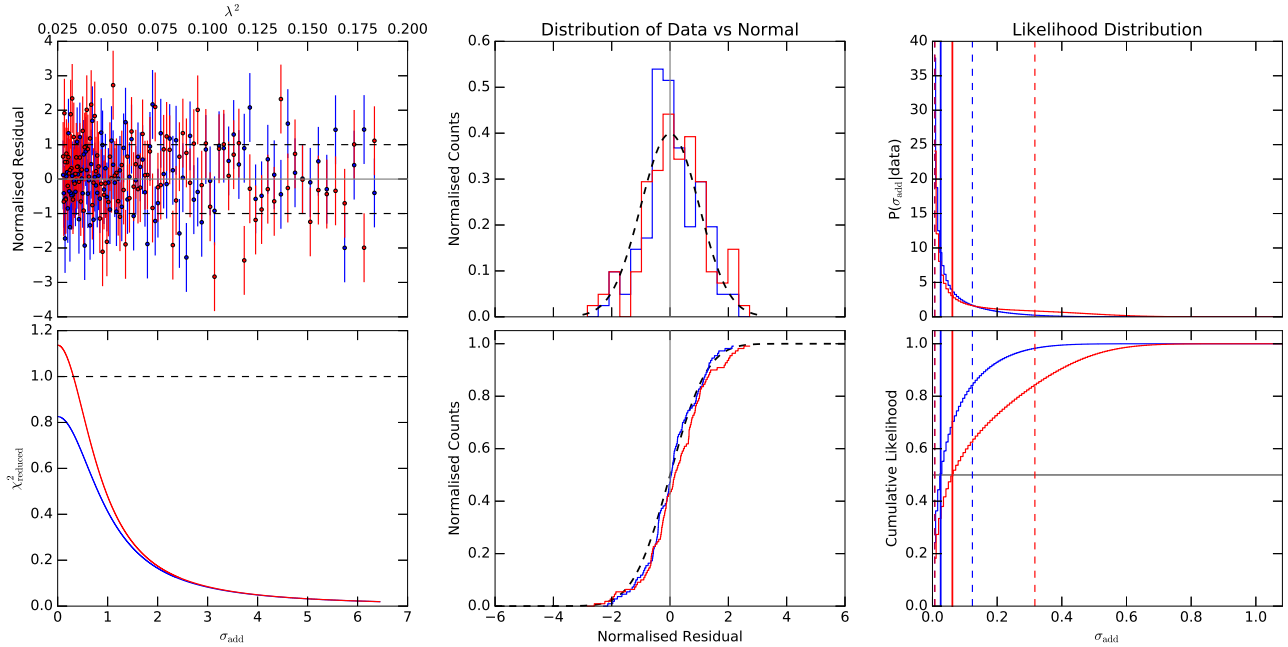

Figure 1: **Top-left:** Residual u/σ_u (blue) and q/σ_q (red) spectra of a simple source after a Faraday thin model derived from RM-synthesis has been subtracted. Dashed lines show the $\pm 1\sigma$ limits. **Bottom-left:** Reduced χ^2 as a function of $\sigma_{\rm add}$. Values < 1 indicate that introducing a significant $\sigma_{\rm add}$ would make the residual uncertainties inconsistently large compared to the data. **Middle column:** The distribution of residual values (solid lines) are consistent with a normal distribution (black dashed curve). **Right column:** Marginal posterior probability distributions for the additional scatter term $\sigma_{\rm add}$. Solid vertical lines shows the mean of the distribution and dashed vertical lines show the $\pm 1\sigma$ values. In this case the most likely values are $\sigma_{\rm add,q} = 0.03^{+0.10}_{-0.02}$ and $\sigma_{\rm add,u} = 0.06^{+0.26}_{-0.06}$, i.e., consistent with zero.

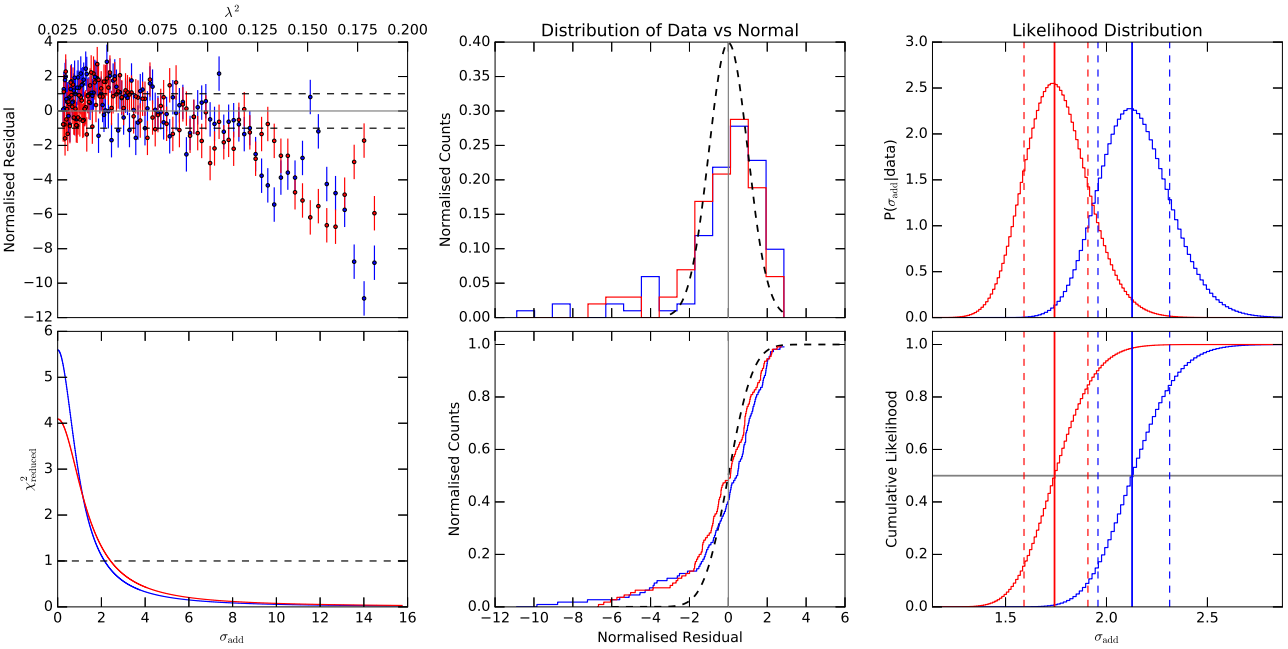

Figure 2: As per Fig. 1, except for a Faraday complex source. The distribution of residual values is inconsistent with being drawn from a normal distribution. Additional scatter terms of $\sigma_{\rm add,q} = 2.13^{+0.19}_{-0.17}$ and $\sigma_{\rm add,u} = 1.74^{+0.17}_{-0.15}$ are required to model the data.

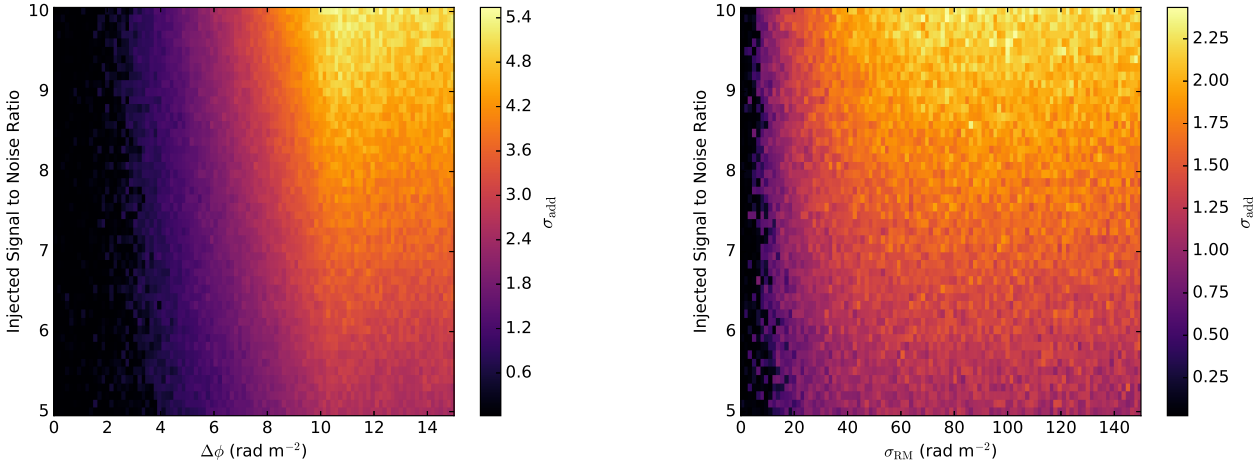

Figure 3: **Left:** Plot of $\sigma_{\rm add} = \max(\sigma_{{\rm add},q},\ \sigma_{{\rm add},u})$ measured from artificial data containing two Faraday thin components separated by $\Delta\phi$ rad m^{-2}. The separation of the components increases along the X-axis. Both components have equal polarised intensities and the signal-to-noise ratio increases along the Y-axis. Values for $\sigma_{\rm add}$ vary smoothly from $\Delta\phi \gtrsim 5\,{\rm rad\,m^{-2}}$ meaning that complexity is detectable at separations significantly smaller than the width of the spread function (FWHM=22.25 rad m^{-2}), even at low signal-to-noise ratios. **Right:** As per the left panel, except the test data contains a single Faraday component affected by increasing amounts of depolarisation following the law of Burn (1966). Faraday dispersion $\sigma_{\rm RM}$ increases from zero along the X-axis and can be detected at values $\sigma_{\rm RM} \gtrsim 20\,{\rm rad\,m^{-2}}$ for weak polarised signals.

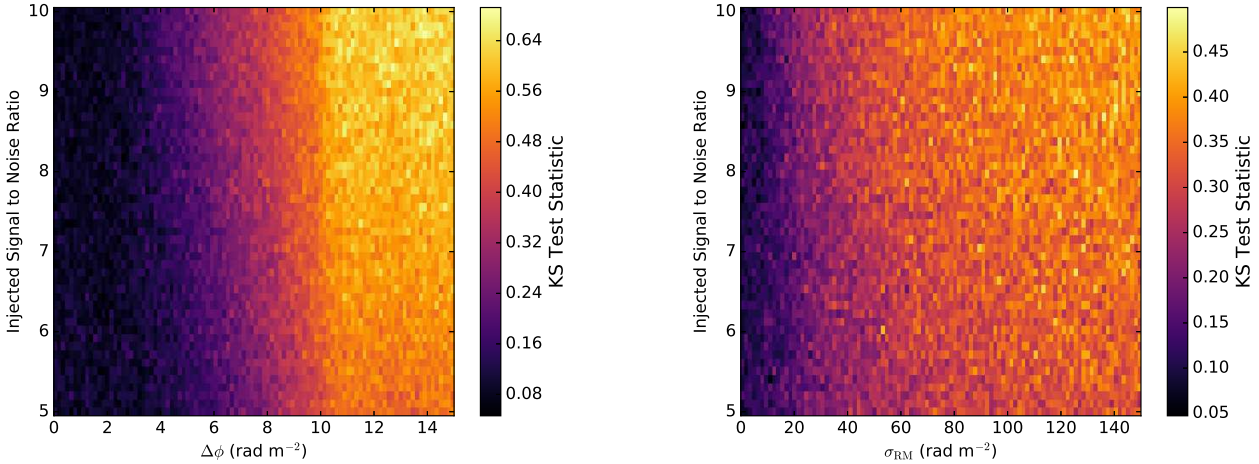

Figure 4: Plots of the KS-statistic for the same grids of models used to make Fig. 3. The KS-test is noisier and generally less sensitive than calculating the most likely value of $\sigma_{\rm add}$.

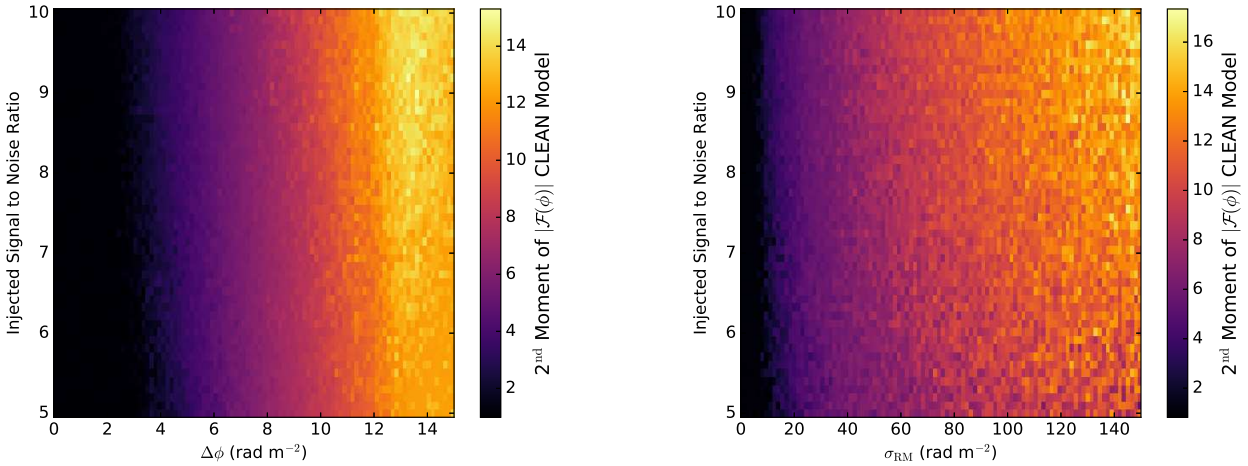

Figure 5: Maps of the 2$^{\rm nd}$ moment of the CLEAN component spectrum of $|\mathcal{F}(\lambda^2)|$ for the same grids of models used to make Fig. 3.

3.2 Detecting Complexity in $\mathcal{F}(\phi)$

Complexity in the FDF can also be assessed by measuring the spread or dispersion of $|\mathcal{F}(\phi)|$ compared to the Rotation Measure Spread Function $\mathcal{R}(\phi)$. This is accomplished by using the Hogbom CLEAN algorithm to deconvolve $|\mathcal{F}(\phi)|$, producing a complex CLEAN component model $\mathcal{F}_m(\phi)$ (e.g., Heald 2009) and then calculating the 2$^{\rm nd}$ moment of $|\mathcal{F}_m(\phi)|$ according to

$$M_2 = \sqrt{\frac{\sum_i^N |\mathcal{F}_{m,i}|\,(\phi_i - \bar{\phi})^2}{\sum_i^N |\mathcal{F}_{m,i}|}}, \tag{6}$$

where $\bar{\phi}$ is the polarisation weighted mean Faraday depth. This method was proposed in a POSSUM technical memo by Brown (2011) and used very successfully by Anderson et al. (2015) in a broad-band survey of 563 extragalactic radio sources. Anderson et al. (2015) also investigated the effect of CLEANing to different threshold values above the measured noise and concluded that this method is reliable above 5σ.

4 Testing the Complexity Metrics

We have tested the ability of our proposed metrics to detect complexity using two types of model: (1) two interfering, unresolved Faraday components and (2) a Burn depolarisation model. The degree of complexity in both models is dependent on only a single parameter allowing us to assess the performance of our methods over a range of signal-to-noise (S/N) values.

Fig. 3 shows how the $\sigma_{\rm add}$ complexity metric behaves for spectra with $5 < {\rm S/N} < 10$, containing 300 channels sampled at 1 MHz intervals between $700 \leq \nu \leq 1800$ MHz. The colour-scale on the maps for both models varies smoothly, with no discontinuities at low S/N or complexity. We believe $\sigma_{\rm add}$ is an excellent indicator of a non-Gaussian residual. The Kolmogorov-Smirnov (KS) test is also very commonly used to assess if a set of samples are likely drawn from a normal distribution. As a comparison, in Fig. 4 we plot the value of the Kolmogorov-Smirnov test statistic for the same grid of models. The KS-test is known to be insensitive, especially when differences are found only in the tails of the distributions. The colour-scale maps in Fig. 4 are clearly subject to more scatter than $\sigma_{\rm add}$ in Fig. 3.

Fig. 5 shows the how the M_2 measurement behaves for the same grid of models. The values for M_s vary smoothly for both types of model and exhibit similar sensitivity as the $\sigma_{\rm add}$ metric.

5 Discussion

The following points are suggested for discussion by the SG5 and SG8 teams:

- **The effect of a poorly fit Stokes *I* spectrum.** Significant structure remaining in Stokes *I* residual could masquerade as Faraday complexity after creating the fractionally polarised spectra. Jointly fitting a spectral-curvature and polarisation model to Stokes *I*, *Q* & *U* would be a more correct thing to do (see Schnitzeler & Lee 2017). However, CSIRO will not do this for the basic POSSUM Polarisation Catalogue.
- **The effect of uneven sampling in λ^2 space.** The $\sigma_{\rm add}$ method is essentially a more robust version of the KS-test and collapses residual into a distribution - i.e., it averages across the pass-band. The flat sampling in frequency space means that channels cluster towards the short wavelength end of the spectrum. Greater sensitivity to λ^2-dependent complexity could be achieved by calculating $\sigma_{\rm add}$ in a window at the long λ^2 end of the spectrum. Alternatively, some sort of weighting could be imposed proportional to the density of samples in λ^2 space.

6 Summary

We have compared three different methods for assessing complexity in Faraday-active spectra at radio wavelengths. We find that our likelihood-based method for detecting spectral deviations from Faraday thin behaviour is comparable to the previously used method of measuring dispersion in a CLEAN component spectrum.

Further development is necessary to mitigate or detect the effect of poor Stokes *I* models and uneven λ^2 sampling.

References

Allison, J. R., Moss, V. A., Macquart, J.-P., et al. 2017, Monthly Notices of the Royal Astronomical Society, 465, 4450

Anderson, C. S., Gaensler, B. M., Feain, I. J., & Franzen, T. M. O. 2015, Astrophysical Journal, 815, 49

Brentjens, M. A., & de Bruyn, A. G. 2005, A&A, 441, 1217

Brown, J. C. 2011, Internal POSSUM Report 9: Assess Complexity of RM Synthesis Spectrum, Tech. rep.

Burn, B. J. 1966, Monthly Notices of the Royal Astronomical Society, 133, 67

Farnes, J. S., Gaensler, B. M., & Carretti, E. 2014, Astrophysical Journal Supplemental Series, 212, 15

Heald, G. 2009, in IAU Symposium, Vol. 259, Cosmic Magnetic Fields: From Planets, to Stars and Galaxies, ed. K. G. Strassmeier, A. G. Kosovichev, & J. E. Beckman, 591–602

Purcell, C. R., Gaensler, B. M., Sun, X. H., et al. 2015, Astrophysical Journal, 804, 22

Schnitzeler, D. H. F. M., & Lee, K. J. 2017, Monthly Notices of the Royal Astronomical Society, 466, 378

Sokoloff, D. D., Bykov, A. A., Shukurov, A., et al. 1998, Monthly Notices of the Royal Astronomical Society, 299, 189

Tribble, P. C. 1991, Monthly Notices of the Royal Astronomical Society, 250, 726